ACS Sustainable Chemistry & Engineering

Research Article

pubs.acs.org/journal/ascecg

Synthesis, Structural, and Morphological Characterizations of Reduced Graphene Oxide-Supported Polypyrrole Anode Catalysts for Improved Microbial Fuel Cell Performances

G. Gnana kumar,*[,†] C. Joseph Kirubaharan,[†] S. Udhayakumar,[†] K. Ramachandran,[†] C. Karthikeyan,[†] R. Renganathan,[‡] and Kee Suk Nahm*[,§]

[†]Department of Physical Chemistry, Madurai Kamaraj University, Madurai-625 021, Tamilnadu, India

[‡]School of Chemistry, Bharadhidasan University, Trichy-620 024, India

[§]School of Chemical Engineering and Department of Hydrogen Fuel Cell Engineering, Chonbuk National University, Jeonju-561-756, Republic of Korea

ABSTRACT: The conductive polypyrrole (PPy)/reduced graphene oxide (rGO) composites were synthesized through simple, environmentally benign, time and cost efficient, in situ polymerization and bioreduction techniques. The pyrrole monomer effectively adsorbed over the negatively charged GO sheets through electrostatic and $\pi-\pi$ interactions was polymerized into polypyrrole in its adsorbed state. The obtained morphological images of the rGO/PPy composite ensured that the entire surface of the active carbon support was covered by PPy. The removal of oxygen functionalities from GO with the aid of *Ocimum tenuiflorum* extract was ascertained through FT-IR and UV−vis absorption spectroscopic studies. The rGO/PPy composite exhibited higher electrocatalytic oxidation current as evidenced from the cyclic voltammetric analysis. The number of actives sites and continuous carrier channels of the rGO/PPy composite exhibited a maximum MFC power density of 1068 mW/m^2, which is almost two-fold higher than that of bare PPy. The strong active carbon support prohibited the swelling and shrinkage of the conductive polymer PPy and provided the strong physico and electrochemical robustness of the rGO/PPy composite, which increased the MFC durability performances up to 300 h. These findings have not only provided fundamental knowledge on the preparation rGO-based composites through a green approach but also have found possible applications in large-scale green energy devices.

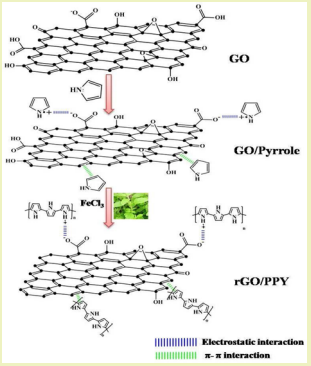

KEYWORDS: *Carbon support, Conduction paths, Electrical conductivity, Oxidation current*

INTRODUCTION

Microbial fuel cells (MFCs) are emerging green energy devices that can use bacterial metabolism for the generation of electrical current from a broad range of organic substrates.[1−3] In MFCs, biomass energy is directly converted into electrical energy via an electron transfer process under an ambient temperature. The development of efficient anode catalysts that could improve the power production of MFCs is highly significant.[4,2] An MFC anode amendment has been extensively developed to increase the bacterial adhesion and electron transfer from bacteria to the electrode surface.[5] A number of electrode materials such as carbon cloth, carbon paper, carbon felt, carbon mesh, stainless steel, graphite, titanium, silver, stainless steel, aluminum, and nickel have been exploited for the green power generation of MFCs.[6−10] Among the studied electrode materials, carbon cloth is well known for its elevated chemical and physical stabilities under an aqueous environment, prompt electrical conductivity, stability, high specific surface area, and porosity. However, the improvement of electron transfer efficiency of carbon cloth is essential in which electrode modification by the conducting polymers is significant.[2] Conducting polymers such as polypyrrole (PPy),[11] polyaniline,[12] polythiophene,[13] poly(aniline-*co*-o-aminophenol),[14] PPy/anthraquinone-2,6-disulfonic disodium salt,[15] poly(3-hydroxy butyrate-*co*-3-hydroxyvalerate),[16] etc. have been exploited for the anode modification process for effectual MFC performances. Among the studied conducting polymers, PPy has been specifically preferred for anode modification, owing to its easier synthesis and processability, elevated electrical conductivity, redox properties, high specific capacitance, low charge transfer resistance, chemical stability, and biocompatibility.[11,15] The high electrical conductivity and electrocatalytic activity of PPy even under neutral solution favors the entrapment of biocatalysts, which increases its viable applications in MFCs.

Hence, few research efforts have been devoted to the modification of anodes by PPy for the application of MFCs.[11,15,17] The conductive polymer PPy-equipped photosynthetic MFC exhibited a power density of 3.4 mW/m^2, and the obtained performance was ascribed to the physical interaction or intercalation of PPy chains into the cell membranes, enabling direct and fast transfer of electrons.[11] The conductive PPy modified with anthraquinone-2,6-disul-

Received: April 10, 2014
Revised: August 18, 2014
Published: September 5, 2014

phonic disodium salt has also been exploited for electricity generation of MFCs, and the obtained concrete MFC performances were attributed to increased bacterial adhesion over the anode surface.[15] Chi et al. modified graphite felt with nanoPPy through the electrosynthesis technique, and the synthesized PPy exhibited a MFC power density of 430 mW/m^2, owing to its elevated conductivity values.[17] However, PPy exhibited certain constraints of lower electrical conductivity, swelling, shrinkage, poor stability, and sluggish electron transfer properties, which limited its maximum MFC performances. The aforementioned limitations of PPy could be effectively tackled by reinforcing the stability of PPy with the active carbon support.[18] It is expected that the electrical conductivity and capacitance of PPy could be increased with the high surface area of an active carbon support.

Graphene is a two-dimensional single atom thick sheet of sp^2 hybridized carbon atoms arranged in a honeycomb lattice, which exhibits superior electrical, mechanical, thermal, and chemical properties.[19] Graphene oxide (GO) is an important derivative of graphene that contains heavily oxygenated graphene sheets bearing epoxy and hydroxyl functional groups on their basal planes and carbonyl and carboxyl groups on the sheet edges.[20] The presence of the aforementioned oxygen moieties in GO imparts a hydrophilic character and provides versatile high volume processing possibilities. However, the hydrophilic functional groups collectively disrupt the conjugated sp^2 network of the basal plane of the individual graphene sheets and degrade the electrical properties of GO.[21] The electrical conductivity of GO sheets can be enhanced by the removal of oxygen functional groups via the reduction process, resulting in reduced graphene oxide (rGO) sheets. For the effective reduction of GO, reducing agents such as hydrazine hydrate, hydroquinone, sodium borohydride, and hydrogen sulfide have been extensively exploited.[22] However, the aforementioned reducing agents exhibit certain limitations such as toxic gas generation, attachment of elemental nitrogen atoms, and incomplete removal of oxygenated species, which hindered the application of rGO in MFCs. Hence, there is a great challenge to develop a green, low-cost, and efficient method for the reduction of GO. Recently, photosynthetic autotroph-mediated nanoparticles preparation grabbed the attention of the green chemistry sector in which the attraction of *Ocimum tenuiflorum* is significant. *Ocimum tenuiflorum* belongs to the *Lamiaceae* family, possessing numerous medicinal properties, and is extensively used in siddha and Ayurvedic medicines. The significant constituents of organic compounds such as oleanolic acid, rosmarinic acid, ursolic acid, eugenol, carvacrol, linalool, β-caryophyllene, β-elemene, and germacrene that exist in the *Ocimum tenuiflorum* extract are useful in decreasing the blood glucose level, promoting the immune system function, and have anticancer, antifertility, antidiabetic, antifungal, hepatoprotective, cardioprotective, analgesic, and adaptogenic properties, along with diaphoretic actions, skin care relief from respiratory disorders, and relief from asthma, fever, lung disorders, and heart diseases.[23−26] In addition, *Ocimum tenuiflorum* contains a variety of phytochemical compounds such as phenols, triterpenes, amino acids, flavones, and eugenol that are found to have strong reduction tendencies,[24] which may be responsible for the reduction of GO.

The polymer/GO/rGO composites are a new class of hybrid materials that exhibits superior physical, mechanical, and electrical properties over their individual counter parts.[27−30] If PPy is interfaced with GO/rGO, electrical conductivity and reinforcement stability of PPy could be improved, which may be beneficial for MFC performances. The unique properties of PPy/GO/rGO composites are purely dependent upon the strong coordination interaction of PPy with GO/rGO sheets, which may strongly influence MFC performances. The main objective of this work is to explore innovative techniques for the preparation of rGO-based composites and to find possible applications as anode catalysts in MFCs.

EXPERIMENTAL SECTION

Materials. Graphite powder, pyrrole, ferric chloride ($FeCl_3$), 2-hydroxy-l,4-naphthoquinone (HNQ), ferricyanide PTFE (60 wt.%), and phosphate buffer saline (PBS) were obtained from Aldrich and used without any further purification. The *Ocimum tenuiflorum* leaves were obtained from local premises. The carbon cloth electrodes obtained from Electrosynthesis Co., Inc., Lancaster, NY. GC-14 was pretreated with ethanol and water and dried in a vacuum oven at 60°C.

Preparation of *Ocimum tenuiflorum* Extract. The fresh *Ocimum tenuiflorum* leaves were finely cut into small pieces and washed with deionized water and dried under an air atmosphere. For the preparation of 10 wt % extract, an appropriate amount of *Ocimum tenuiflorum* leaves was boiled in deionized water for 10 min and cooled to room temperature. The solution was filtered by using Whatmann filter paper, and the obtained *Ocimum tenuiflorum* extract was cooled at 4 °C overnight prior to use.

Synthesis of PPy. The synthesis of PPy was adopted from the procedures as described elsewhere.[31,32] An amount of 0.1 M $FeCl_3$ was added to 0.2 M distilled pyrrole and magnetically stirred for 24 h at room temperature. The obtained polymer was collected via centrifugation and washed several times with a water and ethanol mixture to remove the excess $FeCl_3$. The as-synthesized polymer was dried under vacuum at 60 °C for 24 h.

Synthesis of GO/PPy composite. GO was prepared from graphite powder by using the modified Hummer's method.[21] An amount of 0.2 M distilled pyrrole dissolved in 30 mL of a deionized water and ethanol mixture was added to the GO dispersion (0.5 mg/mL) and magnetically stirred. This was followed by the addition of 0.1 M $FeCl_3$ into the above mixture and magnetically stirred for 24 h. Finally, the prepared composite was centrifuged and dried under vacuum at 60 °C for 24 h.

Synthesis of rGO/PPy Composite. An amount of 0.2 M distilled pyrrole dissolved in 30 mL of a deionized water and ethanol mixture was added to the GO dispersion (0.5 mg/mL) and magnetically stirred. This was followed by the addition of 0.1 M $FeCl_3$ and 3 mL 10 wt % *Ocimum tenuiflorum* extract into the above mixture and magnetically stirred for 24 h. Then the prepared composite was centrifuged and dried under vacuum at 60 °C for 24 h.

Modification of Anode. The synthesized catalysts were mixed with 1 wt % PTFE solution and ultrasonicated for 30 min. The obtained slurry was loaded over the surface of a carbon cloth (1 cm × 1.5 cm) via a spray technique and dried at 100 °C for 12 h.

Microorganism Cultivation. *Escherichia coli* ATCC 27325 obtained from the American Type Culture Collection (ATCC) was aerobically grown in sterilized Luria−Bertani (LB) medium (10 g/L of glucose, 10 g/L of peptone, 5 g/L of yeast, 10 g/L of NaCl, and pH 7). Then, the *Escherichia coli* cells were inoculated and grew at 30 °C under the sterile liquid medium.

Characterizations. The UV−vis absorption studies of prepared nanostructures were evaluated by using Agilent-8453. The crystalline character of the synthesized nanostructures was ascertained by a Rigaku X-ray powder diffractometer (XRD) with Cu Kα radiation (l = 1.54178 Å). Structural characterization of the prepared nanostructures was examined using a PerkinElmer Fourier transform infrared (FT-IR) spectroscopy in the range of 4000−400 cm^{-1} in KBr pellets. Morphological properties of the prepared nanostructures were ascertained by using Hitachi S-4700 field emission scanning electron microscopy (FE-SEM). The electrical conductivities of the prepared

materials were measured by a four point probe method using an Agilent multimeter, Cleveland, Ohio, U.S.A. The surface areas of prepared nanostructures were measured by using a Belsorp Brunauer–Emmett–Teller (BET) surface area analyzer.

The electrochemical performances of prepared nanostructures were carried out in a CHI-650D analytical system. All the electrochemical measurements were performed by using a three-electrode electrochemical system, in which the bare/modified carbon cloth was used as a working electrode, a Ag/AgCl electrode was used as a reference electrode, and a Pt wire was used as a counter electrode. The three-electrode cell configuration was placed in a 1 M glucose and 300 μM 2-hydroxy-1,4- naphthoquinone (HNQ)-mediated *Escherichia coli* solution, and nitrogen gas was purged into the above mixture to maintain an oxygen-free environment.

The MFC performances of studied anode catalysts were evaluated according to the procedure described elsewhere.[6] For the determination of MFC power output, various resistances (510 kΩ to 120 Ω) were used as external loads, and the corresponding output cell voltages were monitored using a data acquisition system (Agilent multimeter, Cleveland, Ohio, U.S.A.) connected to a personal computer.

RESULTS AND DISCUSSION

UV–Vis Absorption Studies. The UV–vis absorption spectra of studied nanostructures are given in Figure 1. The

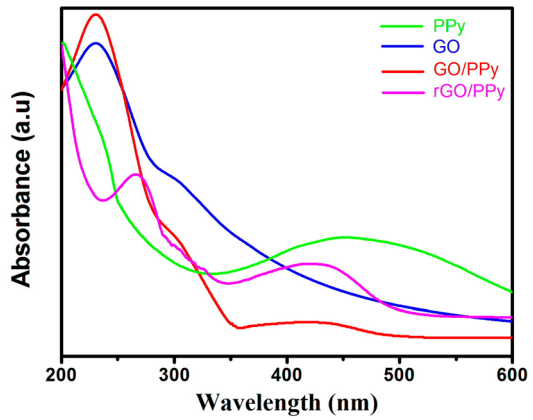

Figure 1. UV–vis absorption spectra of the prepared nanostructures.

π–π* transition of C–C and n–π* transition of C=O bonds of GO are observed from the SPR bands found at 238 and 303 nm, respectively. The characteristic π– π* or polaron absorption band of PPy was found at 450 nm for the bare PPy.[33,34] The existence of carboxyl, carbonyl, epoxy, and hydroxyl functional groups over the surface of GO sheets provided a negative charge to the GO matrix. The positively charged pyrrole was homogeneously adsorbed over the negatively charged GO matrix through electrostatic interaction. The rich aromatic rings in Py are capable of interacting with rGO via π–π stacking (Figure 2). The addition of $FeCl_3$ polymerizes the Py monomer in its adsorbed state and influences the complete coverage of PPy over GO. GO consists of oxygen-containing ether, hydroxyl, epoxide, carbonyl, and carboxyl functional groups,[35,36] which can support the nucleation of a conductive polymer that favors the surface coverage of PPy with the strong π– π interaction between the PPy backbone and GO surface (Figure 2). GO/PPy exhibited three distinctive SPR bands, and the characteristic GO and PPy bands were found at 238 and 303 and 420 nm. rGO/PPy exhibited two SPR bands at 270 and 426 nm, which are ascribed to the π–π* transition of the C–C band of rGO and PPy, respectively.

X-ray Diffraction Patterns. The crystalline structures of the prepared nanomaterials were investigated by XRD, and the corresponding diffraction patterns are shown in Figure 3. The pure PPy exhibited a weak and broad band at 2θ = 24.5^o (Figure 3a), indicating the amorphous structure of a prepared conductive polymer.[37] The obtained diffraction peak corresponds to a *d*-spacing of 0.34 nm, which is associated with the closest distance of planar aromatic pyrrole rings (face-to-face pyrrole rings).[37] In general, the XRD pattern of graphite exhibits a well-defined basal reflection (0 0 2) peak at 2θ = 26.6° with a *d*-spacing value of 0.335 nm.[38,39] The intercalation of water molecules and oxygen-containing functional groups between the layers of graphite increased the *d*-spacing value of GO to 0.86 nm. An intense peak observed at 10.27° represents the (0 0 1) reflection plane, ensuring the formation of GO (Figure 3b).[40] The GO/PPy composite exhibited a broad peak at 25^o, representing the existence of PPy (Figure 3c). Furthermore, the characteristic peak of GO disappeared in the GO/PPy composite, indicating that GO has not exhibited aggregation and was completely used as a substrate for PPy to produce hierarchical nanocomposites. For the rGO/PPy composite, the (0 0 1) reflection plane of GO completely disappeared, ensuring the reduction of GO sheets (Figure 3d), and the appearance of a broad reflection plane at 25.09° confirmed the presence of PPy with the stacked graphene layers of rGO (Figure 3d). The significant features of the XRD pattern of the rGO/PPy composite are similar to pure PPy, ensuring that additional crystalline phases have not been introduced into the composite. The growth of PPy chains in the rGO sheets favored interlayer expansion, and the interplanar spacing of 0.35 nm calculated from the broad peak is identical to the π–π stacking distance, indicating that possible π–π stacking occurred between the PPy chains and rGO planes.

FT-IR Studies. The structural characterization of prepared nanostructures was analyzed by using FT-IR spectroscopy, and the corresponding FT-IR spectra are given in Figure 4. The bands observed at 1556 and 1470 cm^{-1} for PPy (Figure 4a) are attributed to the C–N and C–C stretching vibrations of the pyrrole ring, respectively, which are represented as typical PPy ring vibrations. The C–N stretching band is assigned for the band found at 1310 cm^{-1}.[41] The intensive bands observed at 1198 and 931 cm^{-1} specify the doping state of PPy, and the broad band observed at 3000–3500 cm^{-1} represents the N–H stretching vibration.[41] Figure 4b exhibits the FT-IR spectrum of GO, and the band observed at 1728 cm^{-1} is attributed to the C=O stretching of the carboxylic groups present at the edges of the GO sheets. The C=C stretching vibrations of GO is assigned to the band found at 1634 cm^{-1}. The peaks observed at 1396 and 1096 cm^{-1} represent the C–O stretching vibrations of carboxyl and alkoxy groups, respectively.[42,43] The reduction of GO with the aid of *Ocimum tenuiflorum* extract was ensured from the disappearance of C=O and C–O stretching vibrations (Figure 4c), which confirmed the removal of oxygen functional groups. The presence of PPy in the GO/PPy composite is ensured from the bands observed at 1209 and 1568 cm^{-1}, which are the characteristic peaks of PPy (Figure 4d). The downshifted peaks of PPy in the GO/PPy composite specify that there may be a possible π–π interaction between the GO and PPy rings. The C=O and –OH stretching vibrations at 1728 and 3406 cm^{-1} found for GO (Figure 4b) and GO/PPy (Figure 4d) completely disappeared for the rGO/PPy composite (Figure 4e), representing the complete removal of oxygen functionalities and ensuring the reduction process. In

dx.doi.org/10.1021/sc500244f | *ACS Sustainable Chem. Eng.* 2014, 2, 2283–2290

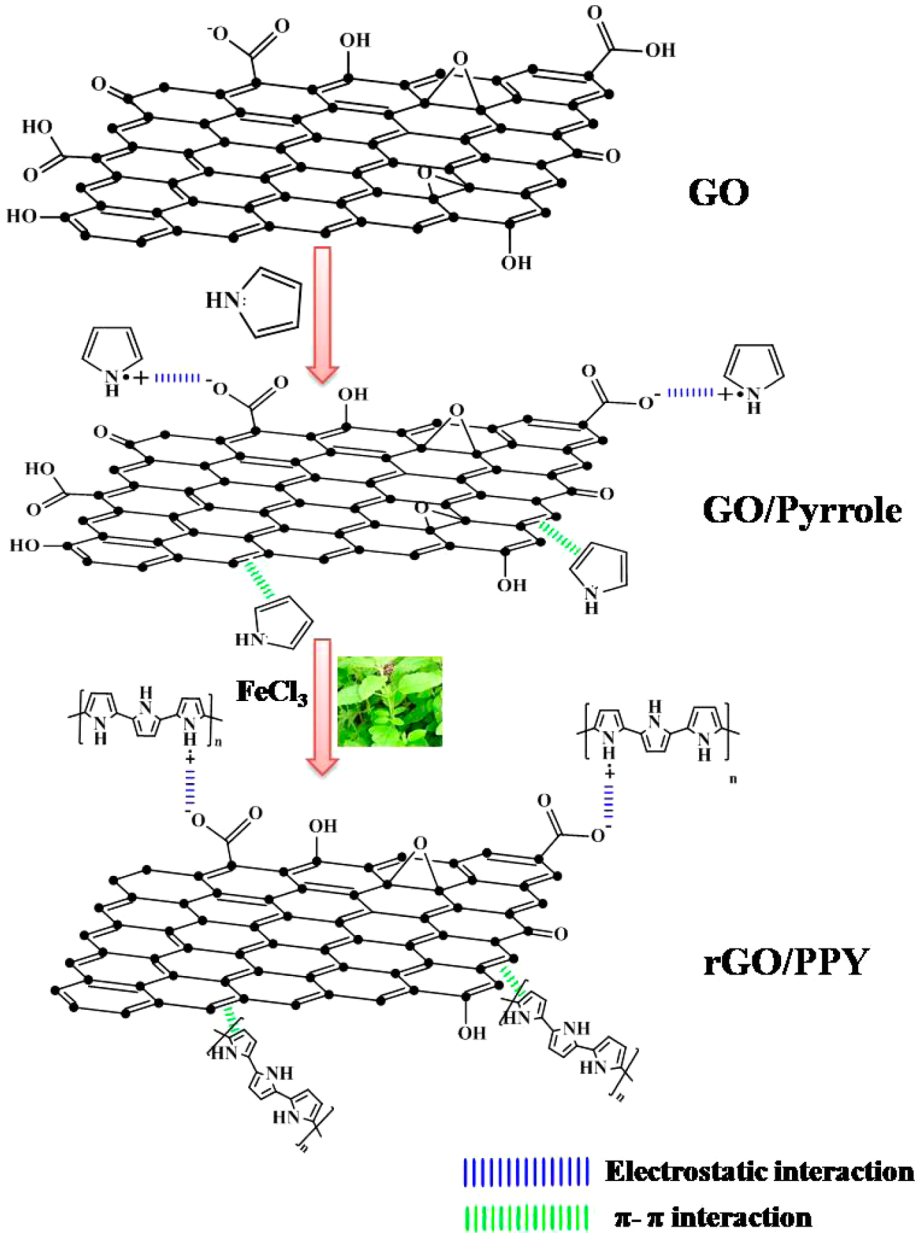

Figure 2. Proposed mechanism for the preparation of the rGO/PPy composite.

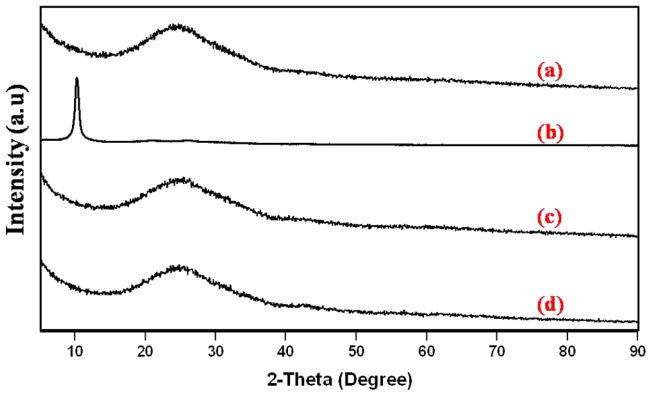

Figure 3. XRD patterns of (a) PPy, (b) GO, (c) GO/PPy, and (d) rGO/PPy.

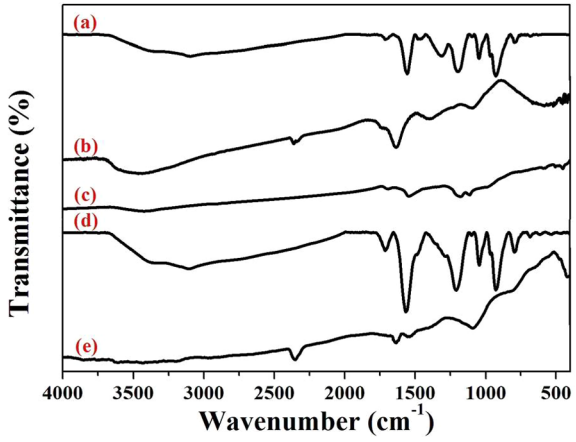

Figure 4. FT-IR spectra of (a) PPy, (b) GO, (c) rGO, (d) GO/PPy, and (e) rGO/PPy.

dx.doi.org/10.1021/sc500244f | ACS Sustainable Chem. Eng. 2014, 2, 2283−2290

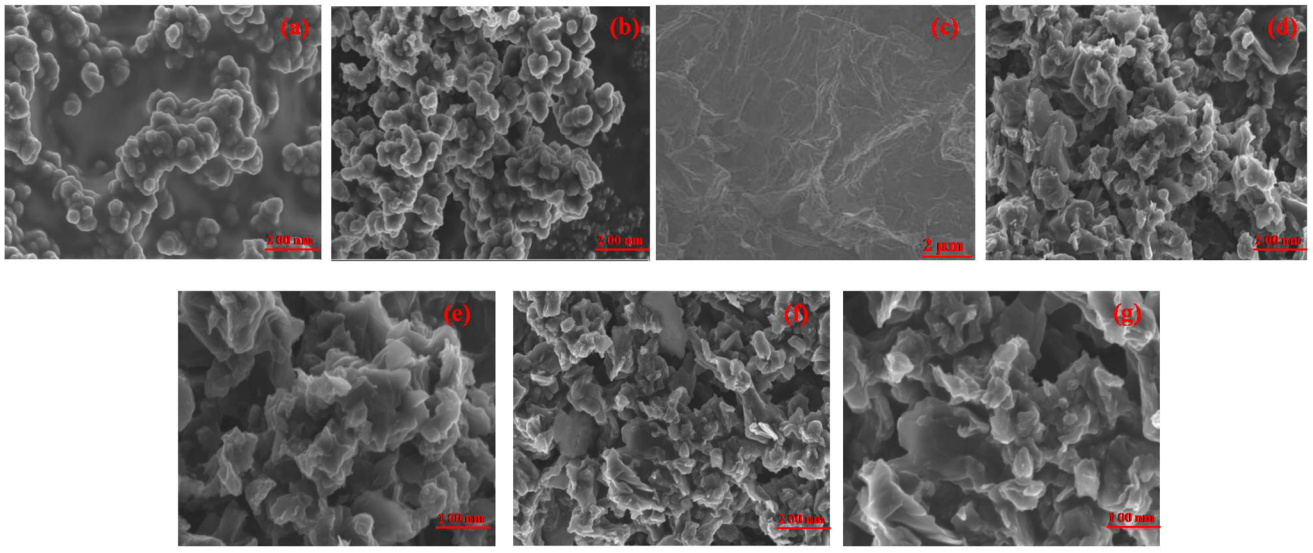

Figure 5. SEM images of (a) and (b) PPy, (c) GO, (d) and (e) GO/PPy, and (f) and (g) rGO/PPy.

addition, the band found at 1635 cm^{-1} is assigned to the amide I bond of proteins arising due to the carbonyl stretch in proteins,[44] which may be responsible for the reduction of GO.

Morphological Properties. The morphological properties of prepared materials were characterized by SEM micrographs and are shown in Figure 5. The PPy exhibited granular like structures with the average particle size of 190 nm as evidenced from Figure 5a and b. The granular like PPy particles are strongly interconnected and exhibited a network-like structure. The polymerization initiated at the interface between two immiscible liquids is responsible for the granular structures of PPy. The bare GO exhibited flat and stacked multilayer sheets as shown in Figure 5c. The granular-like structures disappeared for the GO/PPy composite, and a flaky and rough surface was observed, which is attributed to the polymerization of PPy over the GO sheets (Figure 5d,e). The wrinkled graphene sheets associated with the coverage of PPy was observed for the rGO/PPy composite as shown in Figure 5f and g.

The electrical conductivity and surface area of synthesized PPy are found to be 0.17 S/cm and 11 m^2/g, respectively. The effective restoration of the conjugated π system through the reduction of GO was ensured by the rGO nanosheet's increased electrical conductivity and surface area of 21 S/cm and 120 m^2/g, respectively, which is much higher than the electrical conductivity (1×10^{-5} S/cm) and surface area (26 m^2/g) of GO sheets. The active carbon GO-supported PPy exhibited an improved electrical conductivity and surface area of 2.50 S/cm and 76 m^2/g, respectively, and the improved electrical conductivity and surface area are attributed to the synergisitic effect of PPy with GO. The electrical conductivity and surface area were further increased to 5.36 S/cm and 102 m^2/g, respectively, for the rGO/PPy composite, owing to the smaller size of rGO domains and better graphitization. The obtained electrical conductivity and surface area values are comparable with the chemically reduced GO/PPy nanocomposites as reported elsewhere.[45,46]

Electrochemical Analysis. Cyclic voltammetry (CV) studies were performed to analyze the electrocatalytic activities of prepared nanostructures, and the CV plots of the studied electrodes recorded with a mixture of *Escherichia coli*, 300 μM HNQ, and 1 M glucose at a scan rate of 50 mV/s are given in Figure 6. The minimum oxidation current (Figure 6a) was observed for bare carbon cloth due to its limited electrical

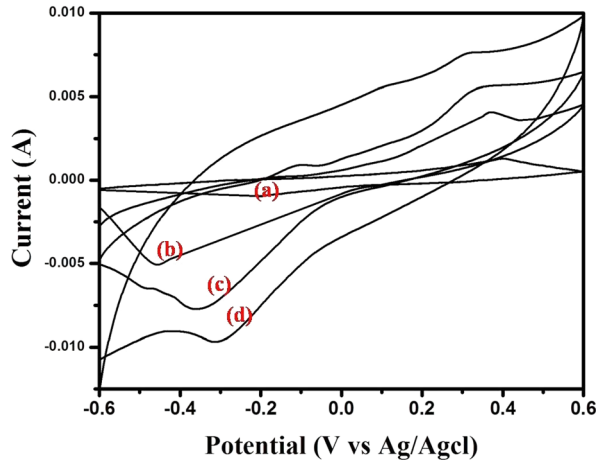

Figure 6. Cyclic voltammograms of (a) unmodified, (b) PPy-, (c) GO/PPy-, and (d) rGO/PPy-modified carbon cloth obtained under *E. coli*, HNQ, and glucose at a scan rate of 50 mV/s.

conductivity. The electrocatalytic oxidation current of carbon cloth was improved by PPy (Figure 6b), owing to its elevated electrical conductivity, number of carriers, and charge carrier mobility (Figure 6b). GO has provided a strong platform for the effectual polymerization of PPy and paves the continuous electron channels for the GO/PPy composite.[47] The effectively polymerized PPy over the GO sheets decreased the electron and mass transfer resistances and increased the contact possibility between electrode and microorganisms, which collectively increased the oxidation current (Figure 6c). The oxygen functionalities that are responsible for the lower electrical conductivity of GO were completely removed for rGO, resulting in high electrical conductivity for the rGO/PPy composite. The high electrical conductivity and extended surface area of the rGO/PPy composite facilitates the bacteria catalytic oxidation of glucose and resulted in the maximum oxidation current (Figure 6d). The observed larger anodic peak current represents higher glucose oxidation.

dx.doi.org/10.1021/sc500244f | ACS Sustainable Chem. Eng. 2014, 2, 2283−2290

MFC Performances. The fuel cell performances of prepared anode catalysts were investigated in a dual chamber MFC, and the obtained results are given in Figure 7. The bare

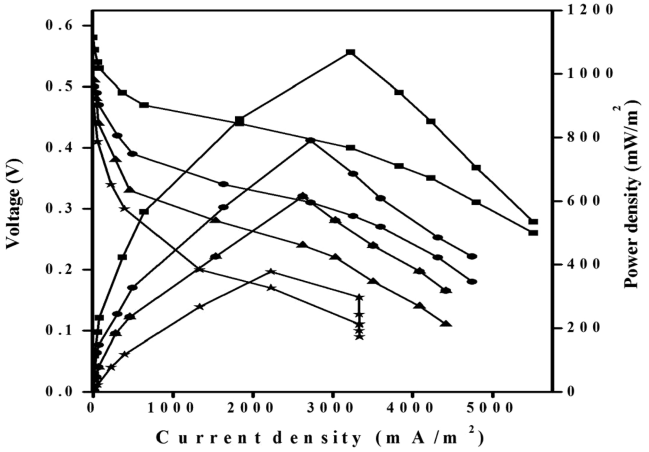

Figure 7. Fuel cell performances of MFC equipped with (★) unmodified, (▲) PPy-, (●) GO/PPy-, and (■) rGO/PPy-modified carbon cloth.

carbon cloth exhibited an inferior power density (377 mW/m^2) among the studied electrodes, owing to its limited conductivity. The MFC performance of the bare carbon cloth was improved by the conductive polymer PPy, and a maximum power density of 615 mW/m^2 was obtained for the PPy-equipped MFC. The nondegenerate conduction band in the ground state and polaron and bipolarons are the dominant charge carriers of PPy. The charge transport along the polymer chains and hopping of carriers are responsible for the elevated electrical conductivity of PPy.

The improved MFC performance is also attributed to the number of conduction paths, longer conjugation length, structural order, and fewer structural defects of the conducting polymer PPy. The GO/PPy reduced the diffusion and migration length and facilitated the electron transfer rate due to the additional charge carriers of the GO sheets.[48,49] The synergistic effect exerted between the conductive polymer and carbon support has also played a vital role in the improved MFC performances. By the combined efforts of the above, GO/PPy exhibited improved power density of 791 mW/m^2. Although the GO/PPy composite exhibited improved MFC performances over PPy, the obtained performance is still inferior for real time applications, owing to the limited electrical conductivity of GO. The substantial increment in electrical conductivity of anode catalysts could bring forth maximum MFC performances and thereby the real time applications of MFC can be guaranteed. This was effectively achieved through the complete removal of the hydrophilic functional groups of GO. The rGO/PPy composite exhibited maximum MFC performances among the studied catalysts, and the observed maximum power density is 1068 mW/m^2. The better graphitization of the C═C bond, π-conjugation of the graphene basal plane, low structural defect density, high aspect ratio, and number of sp^2 domains predominantly determined the high MFC performances of the rGO/PPycomposite.[50,51] The large surface area obtained for the prepared rGO/PPy composite increased the intimate contact between the electroactive species present in microorganisms and the electrode surface, and thereby the charge transfer efficiency and cell−material interaction were facilitated. The continuous conduction pathways provided by the PPy nanoparticles and effective percolative conducting bridges of rGO sheets increased the fast charge transfer rate and high rate capacity of the rGO/PPy composite. The positive charges delocalized in polarons (3−4 pyrrole units) of PPy can move over the polymeric backbone chains and construct the PPy electron conductive.[52] The exposed positively charged PPy in the rGO/PPy composite enhanced the adhesion of a negatively charged bacteria surface via electrostatic interaction, favoring biofilm formation, and therefore, direct and facile electron transfer was facilitated. By the collective efforts of the above, the rGO/PPy composite exhibited improved interfacial properties between electrolyte and electrode, and therefore, maximum MFC performances were facilitated for the rGO/PPy composite.

Durability Studies. For the determination of electrochemical stabilities of prepared nanocatalysts, open circuit voltages (OCV) of the studied catalyst-equipped MFCs were examined as a function of time under a constant load mode with an external resistance of 1000 Ω (Figure 8). When the cell

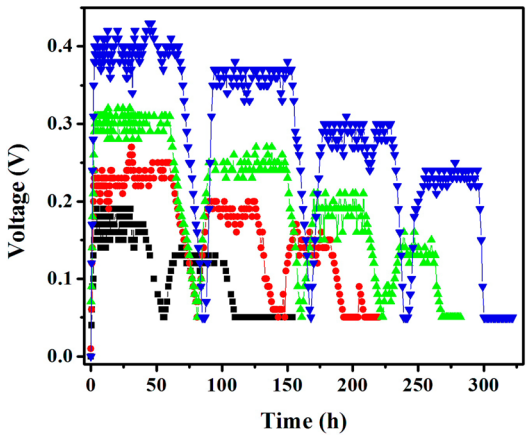

Figure 8. Representative cell voltage−time profile of MFC equipped with (■) bare carbon cloth and (●) PPy-, (▲) GO/PPy-, and (▼) rGO/PPy-modified carbon cloth anodes.

voltage of studied MFCs dropped to 0.05 V, the fresh inoculum was replaced. Although the PPy-modified electrode exhibited the improved durability performances over bare carbon cloth, the obtained durability is still inferior, owing to the swelling, shrinkage, and cracks of PPy and decreased conductivity and surface area of the electrode under repetitive cycles. Among the studied electrocatalysts, rGO/PPy exhibited a maximum MFC durability of more than 300 h. The complete removal of oxygen functionalities from GO favors the hydrophobic character of rGO/PPy that can easily detach the water molecules and maintain the exposed surface area of electrodes under repetitive cycles. In addition, the rGO matrix stabilized the PPy chains and delayed the destroying process of PPy chains from swelling and shrinking during the long-term operation. The prepared rGO/PPy composite exhibited both physio and electrochemical advantages of high mechanical strength and excellent electrical conductivity, respectively, which may prohibit the destruction of an electrode material. The maximum OCV of 0.4 V was obtained at 3 h, and concrete OCVs were maintained for a couple of cycles, which influence the potential application of the prepared composite in MFCs. The biomass accumulated over the surface of the carbon cloth hindered the diffusion of

electrons and also is responsible for the activation resistance per surface area, which collectively decreased the cell voltage of MFC after 300 h.

CONCLUSION

A simple approach has been proposed for the preparation of rGO/PPy nancomposite through simultaneous polymerization and reduction processes. The presence of amide bonds of proteins in *Ocimum tenuiflorum* extract is responsible for the reduction of GO as evidenced from the FT-IR analysis. The electrical conductivity of bare carbon cloth was improved by the PPy nanostructures and was further promoted by active carbon-supported GO and rGO. The high electrical conductivity of the rGO/PPy composite increased the electron transfer efficiency and increased the intimate contact between the microorganisms and electrode. By the combined efforts of high electrical conductivity and number of catalytic active sites, the rGO/PPy composite harvested a number of electrons and exhibited maximum MFC performances. The robust stability stimulated by the active carbon-supported rGO enhanced the durability performances of MFCs for 300 h.

AUTHOR INFORMATION

Corresponding Authors

*E-mail: kumarg2006@gmail.com (G.G.k.). Tel.: 919585752997 (G.G.k.).

*E-mail: nahmks@jbnu.ac.kr (K.S.N.). Fax: +82 63 270 2306 (K.S.N.).

Notes

The authors declare no competing financial interest.

ACKNOWLEDGMENTS

This work was supported by Department of Science and Technology, SERB, New Delhi, Fast Track Project for Young Scientist Grant SR/FT/CS-113/2010(G). This work was supported by the Human Resources Development Programme (No.20114030200060) of the Korea Institute of Energy Technology Evaluation and Planning (KETEP) grant funded by the Korea government Ministry of Trade, Industry and Energy.

REFERENCES

(1) Logan, B. E.; Regan, J. M. Electricity-producing bacterial communities in microbial fuel cells. *Trends Microbiol.* **2006**, *14* (12), 512−518.

(2) Gnana kumar, G.; Sarathi, V. G. S.; Nahm, K. S. Recent advances and challenges in the anode architecture and their modifications for the applications of microbial fuel cells. *Biosens. Bioelectron.* **2013**, *43*, 461−475.

(3) Olivera, V. B.; Simoes, M.; Melo, L. F.; Pinto, A. M. F. R. Overview on the developments of microbial fuel cells. *Biochem. Eng. J.* **2013**, *73*, 53−64.

(4) Qiao, Y.; Li, C. M.; Bao, S. J.; Bao, Q. L. Carbon nanotube/polyaniline composite as anode material for microbial fuel cells. *J. Power Sources.* **2007**, *170* (1), 79−84.

(5) Zhao, F.; Rahunen, N.; Varcoe, J. R.; Chandra, A.; Rossa, C. A.; Thumser, A. E.; Slade, R. C. T. Activated carbon cloth as anode for sulfate removal in a microbial fuel cell. *Environ. Sci. Technol.* **2008**, *42* (13), 4971−4976.

(6) Ho, P. I.; Gnana kumar, G.; Kim, A. R.; Kim, P.; Nahm, K. S. Microbial electricity generation of diversified carbonaceous electrodes under variable mediators. *Bioelectrochemistry* **2011**, *80* (2), 99−104.

(7) Wang, X.; Cheng, S.; Feng, Y.; Merrill, M. D.; Saito, T.; Logan, B. E. Use of carbon mesh anodes and the effect of different pretreatment methods on power production in microbial fuel cells. *Environ. Sci. Technol.* **2009**, *43* (17), 6870−6874.

(8) Dumas, C.; Mollica, A.; Feron, D.; Basseguy, R.; Etcheverry, L.; Bergel, A. Marine microbial fuel cell: Use of stainless steel electrodes as anode and cathode materials. *Electrochim. Acta* **2007**, *53* (2), 468−473.

(9) Heijne, A. T.; Hamelers, H. V. M.; Saakes, M.; Buisman, C. J. N. Performance of non-porous graphite and titanium-based anodes in microbial fuel cells. *Electrochim. Acta* **2008**, *53* (18), 5697−5703.

(10) Ouitrakul, S.; Sriyudthsak, M.; Charojrochkul, S.; Kakizono, T. Impedance analysis of bio-fuel cell electrodes. *Biosens. Bioelectron.* **2007**, *23* (5), 721−727.

(11) Zou, Y.; Pisciotta, J.; Baskakov, I. V. Nanostructured polypyrrole-coated anode for sun-powered microbial fuel cells. *Bioelectrochemistry* **2010**, *79* (1), 50−56.

(12) Yong, Y. C.; Dong, X. C.; Park, M. B. C.; Song, H.; Chen, P. Macroporous and monolithic anode based on polyaniline hybridized three-dimensional graphene for high performance microbial fuel cells. *ACS Nano* **2012**, *6* (3), 2394−2400.

(13) Vu, Q. T.; Pavlik, M.; Hebestreit, N.; Rammelt, U.; Plieth, W.; Pfleger, J. Nanocomposites based on titanium dioxide and polythiophene: Structure and properties. *React. Funct. Polym.* **2005**, *65* (1−2), 69−77.

(14) Li, C.; Zhang, L.; Ding, L.; Ren, H.; Cui, H. Effect of conductive polymers coated anode on the performance of microbial fuel cells (MFCs) and its biodiversity analysis. *Biosens. Bioelectron.* **2011**, *26* (10), 4169−4176.

(15) Feng, C.; Ma, L.; Li, F.; Mai, H.; Lang, X.; Fan, S. A polypyrrole/anthraquinone-2,6-disulphonic disodium salt (PPy/AQDS)-modified anode to improve performance of microbial fuel cells. *Biosens. Bioelectron.* **2010**, *25* (6), 1516−1520.

(16) Luckarift, H. R.; Sizemore, S. R.; Farrington, K. E.; Roy, J.; Lau, C.; Atanassov, P. B.; Johnson, G. R. Facile fabrication of scalable, hierarchically structured polymer/carbon architectures for bioelectrodes. *ACS Appl. Mater. Interfaces* **2012**, *4* (4), 2082−2087.

(17) Chi, M.; He, H.; Wang, H.; Zhou, M.; Gu, T. Graphite felt anode modified by electropolymerization of nano-polypyrrole to improve microbial fuel cell (MFC) production of bioelectricity. *J. Microbial. Biotechnol.* **2013**, DOI: 10.4172/1948-5948.S12-004.

(18) Razaq, A.; Nyholm, L.; SJodin, M.; Stromme, M.; Mihranyan, A. Paper-based energy-storage devices comprising carbon fiber-reinforced polypyrrole-cladophora nanocellulose composite electrodes. *Adv. Eng. Mater.* **2012**, *2* (4), 445−454.

(19) Choi, W.; Lahiri, I.; Seelaboyina, R.; Kang, Y. S. Synthesis of graphene and its applications: A review. *Crit. Rev. Solid State* **2010**, *35*, 52−71.

(20) Huang, X.; Qi, X.; Boey, F.; Zhang, H. Graphene-based composites. *Chem. Soc. Rev.* **2012**, *41* (2), 666−686.

(21) Hummers, W. S.; Offeman, R. E. Preparation of graphitic oxide. *J. Am. Chem. Soc.* **1958**, *80* (6), 1339−1339.

(22) Compton, O. C.; Jain, B.; Dikin, D. A.; Abouimrane, A.; Amine, K.; Nguyen, S. T. Chemically active reduced graphene oxide with tunable C/O ratios. *ACS Nano* **2011**, *5* (6), 4380−4391.

(23) Zaheer, Z.; Rafiuddin. Bio-conjugated silver nanoparticles: from ocimum sanctum and role of cetyltrimethyl ammonium bromide. *Colloids Surf., B* **2013**, *108*, 90−94.

(24) Patil, R. S.; Kokate, M. R.; Kolekar, S. S. Bioinspired synthesis of highly stabilized silver nanoparticles using Ocimumtenuiflorum leaf extract and their antibacterial activity. *Spectrochim. Acta, Part A* **2012**, *91*, 234−238.

(25) Prakash, P.; Gupta, N. Therapeutic uses of ocimum sanctum linn (tulsi) with a note on eugenol and its pharmacological actions: a short. *Indian J. Physiol. Pharmacol.* **2005**, *49*, 125−131.

(26) Philip, D.; Unni, C. Extracellular biosynthesis of gold and silver nanoparticles using Krishnatulsi (*Ocimum sanctum*) leaf. *Phys. E* **2011**, *43*, 1318−1322.

(27) Stankovich, S.; Dikin, D. A.; Dommett, G. H. B.; Kohlhaas, K. M.; Zimney, E. J.; Stach, E. A.; Piner, R. D.; Nguyen, S. B. T.; Ruoff, R. S. Graphene-based composite Materials. *Nature* **2006**, *442* (7100), 282−286.

(28) Kuila, T.; Bhadra, S.; Yao, D.; Kim, N. H.; Bose, S.; Lee, J. H. Recent advances in graphene based polymer composites. *Prog. Polym. Sci.* **2010**, *35* (11), 1350−1375.
(29) Yang, X.; Li, L.; Shang, S.; Tao, X. M. Synthesis and characterization of layer-aligned poly(vinyl alcohol)/graphene nanocomposites. *Polymer* **2010**, *51* (15), 3431−3435.
(30) Zhang, H. B.; Zheng, W. G.; Yan, Q.; Yang, Y.; Wang, J. W.; Lu, Z. H.; Ji, G. Y.; Yu, Z. Z. Electrically conductive polyethylene terephthalate/graphene nanocomposites prepared by melt compounding. *Polymer* **2010**, *51* (5), 1191−1196.
(31) Vernitskaya, T. V.; Efimov, O. N. Polypyrrole: A conducting polymer; its synthesis, properties and applications. *Russ. Chem. Rev.* **1997**, *66*, 443−457.
(32) Armes, S. P. Optimum reaction conditions for the polymerization of pyrrole by iron (III) chloride in aqueous solution. *Synth. Met.* **1987**, *20*, 365−371.
(33) Hong, T. K.; Lee, D. W.; Choi, H. J.; Shin, H. S.; Kim, B. S. Transparent, flexible conducting hybrid multilayer thin films of multiwalled carbon nanotubes with graphene nanosheets. *ACS Nano* **2010**, *4* (7), 3861−3868.
(34) Borthakur, L. J.; Konwer, S.; Das, R.; Dolui, S. K. Preparation of conducting composite particles of styrene−methyl acrylate copolymer as the core and graphite-incorporated polypyrrole as the shellby surfactant-free mini emulsion polymerization. *J. Polym. Res.* **2011**, *18* (5), 1207−1215.
(35) Luo, Z.; Lu, Y.; Somers, L. A.; Johnson, A. T. C. High yield preparation of macroscopic graphene oxide membrane. *J. Am. Chem. Soc.* **2009**, *131* (3), 898−899.
(36) Gnana kumar, G.; Babu, K. J.; Nahm, K. S.; Hwang, Y. J. A facile one-pot green synthesis of reduced graphene oxide and its composites for nonenzymatic hydrogen peroxide sensor applications. *RSC Adv.* **2014**, *4*, 7944.
(37) Chitte, H. K.; Bhat, N. V.; Walunj, V. E.; Shinde, G. N. Synthesis of polypyrrole using ferric chloride ($FeCl_3$) as oxidant together with some dopants for use in gas sensors. *J. Sensor Technol.* **2011**, *1*, 47−56.
(38) Kuila, T.; Bose, S.; Mishra, A. K.; Khanra, P.; Kim, N. H.; Lee, J. H. Chemical functionalization of graphene and its applications. *Prog. Mater. Sci.* **2012**, *57* (7), 1061−1105.
(39) Machado, B. F.; Serp, P. Graphene-based materials for catalysis. *Catal. Sci. Technol.* **2012**, *2*, 54−75.
(40) Park, S.; An, J.; Potts, J. R.; Velamakanni, A.; Murali, S.; Murali, S.; Ruoff, R. S. Hydrazine-reduction of graphite- and graphene oxide. *Carbon.* **2011**, *49* (9), 3019−3023.
(41) Yang, S.; Shen, C.; Liang, Y.; Tong, H.; He, W.; Shi, X.; Zhang, X.; Gao, H. J. Graphene nanosheets-polypyrrole hybrid material as a highly active catalyst support for formic acid electro-oxidation. *Nanoscale* **2011**, *3*, 3277−3284.
(42) Guo, H. L.; Wang, X. F.; Qian, Q. Y.; Wang, F. B.; Xia, X. H. A green approach to the synthesis of graphene nanosheets. *ACS Nano* **2009**, *3* (9), 2653−2659.
(43) Zhu, C.; Guo, S.; Fang, Y.; Dong, S. Reducing sugar: New functional molecules for the green synthesis of graphene nanosheets. *ACS Nano* **2010**, *4* (4), 2429−2437.
(44) Singhal, G.; Bhavesh, R.; Kasariya, K.; Sharma, A. R.; Singh, R. P. Biosynthesis of silver nanoparticles using *Ocimum sanctum* (Tulsi) leaf extract and screening its antimicrobial activity. *J. Nanopart. Res.* **2011**, *3*, 2981−2988.
(45) Saner, B.; Gürsel, S. A.; Yürüm, Y. Layer-by-layer polypyrrole coated graphite oxide and graphene nanosheets as catalyst support materials for fuel cells. *Fuller. Nanotub. Car.N.* **2013**, *21*, 233−247.
(46) Okan, B. S.; Yürüm, A.; Gorgülü, N.; Gürsel, S. A.; Yürüm, Y. Polypyrrole coated thermally exfoliated graphite nanoplatelets and the effect of oxygen surface groups on the interaction of Pt catalysts with graphene-based nanocomposites. *Ind. Eng. Chem. Res.* **2011**, *50*, 12562−12571.
(47) Konwer, S.; Boruah, R.; Dolui, S. K. Studies on conducting polypyrrole/graphene oxide composites as supercapacitor electrode. *J. Electron. Mater.* **2011**, *40* (11), 2248−2255.
(48) Deng, M.; Yang, X.; Silke, M.; Qiu, W.; Xu, M.; G. Borghs, G.; Chen, H. Electrochemical deposition of polypyrrole/graphene oxide composite on microelectrodes towards tuning the electrochemical properties of neural probes. *Sens. Actuators, B* **2011**, *158* (1), 176−184.
(49) Li, J.; Xie, H. Synthesis of graphene oxide/polypyrrole nanowire composites for supercapacitors. *Mater. Lett.* **2012**, *78* (1), 106−109.
(50) Chandra, V.; Kim, K. S. Highly selective adsorption of Hg^{2+} by a polypyrrole−reduced graphene oxide composite. *Chem. Commun.* **2011**, *47*, 3942−3944.
(51) Liu, Y.; Zhang, Y.; Ma, G.; Wang, Z.; Liu, K.; Li, H. Ethylene glycol reduced graphene oxide/polypyrrole composite for supercapacitor. *Electrochim. Acta* **2013**, *88*, 519−525.
(52) Palmqvist, E.; Kriz, C. B.; Khayyami, M.; Danielsson, B.; Larsson, P. O.; Mosbach, K.; Kriz, D. Development of a simple detector for microbial metabolism based on a polypyrrole dc resistometric device. *Biosens. Bioelectron* **1994**, *9*, 551−556.